Journal Title
XX(X):1–13

DOI: 10.1177/ToBeAssigned
www.sagepub.com/
SAGE

Parametric investigation of a large marine two-stroke dual fuel HPDI engine by using CFD

Renyou Yang[1] , Gerasimos Theotokatos[2] and Dracos Vassalos[2]

Abstract

This study aims at the parametric investigation of the gas injection system settings of a large marine two-stroke dual fuel engine by using a developed and customized CFD method in the ANSYS Fluent software. The investigated engine injection system parameters include the gas injection timing, the gas injection duration, the gas injector lateral angle, and the gas injector holes number. Based on the comparison of the predicted performance parameters for the closed-cycle processes, the results indicate that the gas injector lateral angle is the most significant parameter that affects the engine power as well as the NO and CO_2 emissions. For satisfying the contradictory objectives of retaining the engine power and reducing the NO and CO_2 emissions, appropriate design settings for the gas injection are recommended for the investigated engine operation in the gas mode at 75% load.

Keywords

Marine two-stroke dual fuel engine, High pressure direct gas injection, Gas injection parameters, Parametric investigation, CFD analysis

Introduction

Natural gas, which primarily consists of methane up to 95%, is regarded as a promising alternative greener fuel for marine engines and ships applications due to the advance and availability of the marine duel fuel engines. It has been proved that the natural gas can contribute to the considerable reduction of green-house and non-greenhouse emissions from ship operations, thus reducing the shipping industry environmental footprint. The natural gas combustion characteristics are governed by the methane properties, such as the high octane number (ON). High octane number implies a relatively highly auto-ignition temperature, and therefore, renders the natural gas a suitable fuel for high compression ratio engines, which employ pilot diesel fuel for providing the required ignition energy to enable combustion. The pilot fuel is considered as the ignition kernel in this type of compression ignition (CI) engines.

For the four-stroke dual fuel engines, a number of investigations related to the fuels (pilot and gas) injection settings were conducted. Larson[1] and Imhof et al.[2] experimentally quantified the effects of the relative injection timing (RIT) between the pilot and gas fuels injection starts on the pollutant emissions. Lee and Montgomery[3] performed a numerical analysis demonstrating that a small RIT could cause the increase of the nitrogen oxides (NOx) emissions, whilst not considerably influencing the engine indicated work. In addition, other critical injection parameters, such as the pilot and gas fuels injection timings [1,4–6], the fuels injection profile[7], the fuels injection direction[3,7], and the injectors holes number[3], were investigated either experimentally or by using computational fluid dynamics (CFD) methods.

For the two-stroke marine engines, which have been widely used for the merchant ocean-going ships propulsion, two different dual fuel types, namely the premixed combustion engine and the direct injection engine, have been developed by the marine engine manufacturers. In the former, the natural gas is injected at the mid-stroke cylinder position, which subsequently mixes with the scavenge air during the compression stroke[8]. In the latter, the natural gas is compressed to a high pressure (around 30 MPa) and directly injected into the engine combustion chamber through the gas injectors. In subsequence, the formed mixture of natural gas and air is ignited by using the pilot fuel (injected earlier) ; the combustion is targeted to start close to the cylinder top dead center (TDC)[9]. Owing to the specific combustion characteristics, the knocking and misfiring instabilities can be avoided in the high pressure direct injection (HPDI) dual fuel engines, whereas the carbon dioxide (CO_2), nitrogen oxides (NOx), sulphur oxides (SOx) and particulate matter (PM) emissions can be considerably reduced in comparison with the diesel mode engine operation[10]. According to the engine manufacturer[9], a marine two-stroke dual fuel HPDI engine can operate in the diesel mode (burning diesel fuel oil) or in the gas mode; in the latter, the engine can operate with minimum pilot oil (employing a minimum amount of pilot diesel fuel to start the combustion of the gas fuel) or at a specified dual fuel

[1]Peng Cheng Laboratory, Shenzhen, China
[2]Maritime Safety Research Centre, Department of Naval Architecture, Ocean & Marine Engineering, University of Strathclyde, Glasgow, UK

Corresponding author:
Renyou Yang, Peng Cheng Laboratory, 2 Xingke First Street, Nanshan District, Shenzhen, Guangdong, 518000, China.
Email: yangry@pcl.ac.cn

operation (burning any mixture percentage of diesel fuel and gas fuel).

Experimental studies for investigating the in-cylinder processes in marine engines (of the diesel and dual fuel types) are limited as is extremely challenging to measure the in-cylinder performance parameters (apart from the cylinder pressure) for characterising and analysing the fuel injection, combustion and scavenging processes in these engines. On the other hand, the CFD analysis has been extensively employed for investigating the in-cylinder processes in internal combustion engines due to its advantage on capturing the involved complicated physics and thus estimating the spacial-temporal variations of the in-cylinder performance and emissions parameters. However, this is the first study that investigates the injection and combustion processes in a large marine two-stroke dual fuel engine by using CFD analysis.

The present study focuses on the parametric investigation of a large marine two-stroke dual fuel engine operation at 75% load by using the developed CFD models[11]. The investigated dual fuel injection parameters include the gas injection timing, the gas fuel injection duration, the lateral angle of the gas fuel nozzle and the gas injectors holes number. The effects of these parameters on the engine indicated work and emissions are identified and discussed, whereas the recommendations for the optimal design settings of the gas injection parameters are provided. It must be noted that the gas mode operation with the minimum pilot fuel operation is investigated in this study, denoted as gas mode in the following sections.

CFD model

In this study, one cylinder of the large marine two-stroke HPDI dual fuel engine S60ME-GI[12] is investigated by using CFD analysis. The natural gas is directly injected into the engine combustion chamber close to the top death center (TDC) with a high-pressure ratio (considering the pressure upstream the gas nozzle and the pressure of engine combustion chamber). Due to the high octane number for the natural gas, the pilot liquid fuel is required to be injected, in order to ignite the natural gas.

The closed-cycle operating processes of the investigated engine are simulated by employing the CFD software ANSYS Fluent[13]. The SST k-ω turbulence model[14] is adopted to close the Reynolds-averaged Navier–Stokes (RANS) equations, whereas the Peng–Robinson gas state equation[15] is employed as the working conditions of the mixture in the engine combustion chamber reach the supercritical state. The dynamic mesh method is also used, due to the piston reciprocating motion, as well as the adjustable time steps in the cycle part with the fuels (pilot and gas) injection and combustion processes.

With regards to the pilot fuel injection, the atomizer model with the cone-shaped region in the CFD software ANSYS Fluent[13] is used to simulate the initial injection process. The profiles of the pilot fuel injection velocity and the associated injection rate are estimated by using the Bernoulli equation. The SSD model[16] is employed to simulate the pilot fuel breakup process.

As the high-pressure gas is injected into the engine combustion chamber, the underexpanded flow downstream the gas nozzle and the expansion fan is expected to move towards the high-pressure side inside the gas nozzle, which significantly affects the gas injection and the entrainment with the engine combustion chamber mixture[17,18]. Herein, the pseudo-diameter concept[17] and the 1-D shock tube theory are employed to evaluate such effects, as proposed in Hajialimohammadi et al.[18]. The normal gas injection velocity and the pseudo diameter are calculated by the following equations:

$$\begin{aligned} U_g &= (P_6 - P_\infty)\sqrt{\frac{2}{\rho_\infty[(\gamma_\infty+1)P_6+(\gamma_\infty-1)P_\infty]}} \\ &= \frac{2\sqrt{\gamma_g R_{mg} T_g}}{\gamma_g - 1}\left[1 - (\frac{P_6}{P_g})^{(\gamma_g-1)/2\gamma_g}\right] \end{aligned} \tag{1}$$

$$d_{ps} = d_n\sqrt{\frac{P_6}{P_\infty}} \tag{2}$$

Chocked flow conditions are expected in the gas nozzles due to the high-pressure gas injection. Therefore, the corresponding injected gas mass flow rate and density are calculated by the following equations:

$$\dot{m}_g = \tfrac{1}{4}\pi d_n^2 \rho_g \sqrt{\gamma_g R_{mg} T_g}(\tfrac{2}{\gamma_g+1})^{\frac{2\gamma_g-1}{2(\gamma_g-1)}} \tag{3}$$

$$\rho_{ps} = \rho_g \tfrac{P_\infty}{P_6}\tfrac{\sqrt{\gamma_g R_{mg} T_g}}{U_g}(\tfrac{2}{\gamma_g+1})^{\frac{2\gamma_g-1}{2(\gamma_g-1)}} \tag{4}$$

The developing conserved-equation sources approach[11] is employed to simulate the high-pressure gas injection into the engine combustion chamber. The source terms of the mass, momentum, enthalpy and mixture fraction governing equations, which are used to represent the gas injection into the engine combustion chamber, are described by the following equations, respectively:

$$S_U = \sum \dot{m}_g/\delta V_g \tag{5}$$

$$\vec{F}_U = \sum U_g \dot{m}_g \vec{n}_g/\delta V_g (6) \tag{6}$$

$$S_h = \sum(\int_{T_{ref}}^{T_g} C_{Pg} dT + h_{0g})\dot{m}_g/\delta V_g \tag{7}$$

$$S_Z = \sum \dot{m}_g/\delta V_g \tag{8}$$

The source terms for the turbulent kinetic energy and its dissipation rate are estimated by the following equations, as proposed by Choi et al.[19].

$$S_k = 1.5(U_g^{'})^2 \rho_{ps}/dt \tag{9}$$

$$S_\varepsilon = 0.5[1.5(U_g^{'})^2]^{1.5}\rho_{ps}/(d_n dt) \tag{10}$$

The employed fuels (pilot diesel and gas) combustion models are based on the steady diffusion flamelet model[20]. The pilot fuel combustion process is firstly calculated, in which the combustion kernel parameters including the locations, the diameter and the temperature distributions against the crank angle are estimated. Subsequently, the energy equation source attributed to the pilot fuel combustion

are estimated by using the following equation:

$$S_{ig} = \sum_{k} Y_k [\int_{T_{local}}^{\bar{T}_{ir}} C_{P,k} dT] \quad (11)$$

The high-pressure gas is injected into the engine combustion chamber, where it subsequently ignites by the pilot fuel combustion kernel; this is modelled by introducing the source term S_{ig} in the total enthalpy equation. The associated skeletal chemical kinetics mechanism of the natural gas (methane) is derived from Bilger and Starner[21]. The details of the employed fuels non-premixed combustion models are described in Yang[11].

Validation of the diffusion combustion models

The comprehensive CFD validation of the injection and combustion models for the investigated engine operating in the gas mode was conducted by Yang[11], including the pilot (liquid) fuel injection model, the high-pressure gas injection model, the dual fuel combustion model and the comparison of the derived engine performance with the respective engine operation at the diesel operating mode.

In this section, the experimentally measured parameters in a rapid compression expansion machine (RCEM) reported in Imhof et al.[2] are used to validate the developed pilot and gas fuels injection and combustion models. In addition, the the performance and emission parameters for the dual fuel (DF) and the diesel operations of the RCEM are calculated and compared with the respective experimental measurements from Imhof et al.[2].

Figure 1 depicts the derived heat release rates (HRRs) from the CFD model calculations and the experimentally measured parameters. Based on these results, it can be deduced that the developed models can adequately predict the non-premixed combustion processes for the diesel and the DF modes. The nitrogen monoxide (NO) emissions in the developed models are calculated by employing the extended Zeldovich mechanism according to the recommended reaction rates by Hanson and Salimian[22]. By comparing the derived results with the measured NO emissions as shown in Table 1, it can be inferred that the change of the NO emissions between the DF mode and the diesel mode are sufficiently evaluated by the CFD model, despite of the notable discrepancy up to 38% in the absolute NO fraction values. Similar trends were reported in Schwerdt[23] and Tao et al.[24], in which the errors between the measured and the calculated NO emissions were estimated up to 50% or more.

The HRRs calculated by using the CFD model results for three different cases of the pilot fuel injection timing (early, normal, late) along with the respective experimentally obtained HRRs by Imhof et al.[2] are shown in Figure 2. By comparing the CFD results with the experimental results (Figure 2 and Table 1), it can be inferred that the calculated HRRs as well as the NO emissions variation are of adequate accuracy for the early and normal pilot injection cases.

In the case of the late pilot injection timing, a considerable increase of the peak HRR value is observed in the experimental results. When the pilot injection and the main gas injection timings are close, the liquid fuel ignition is

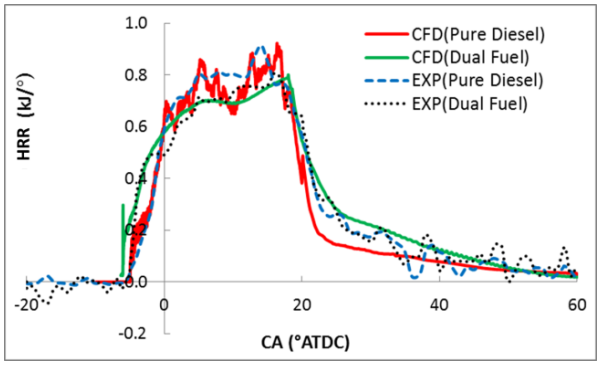

Figure 1. HRRs calculated by the developed CFD models and the experiments conducted by Imhof et al.[2] for the diesel and dual fuel operation in the RCEM chamber.

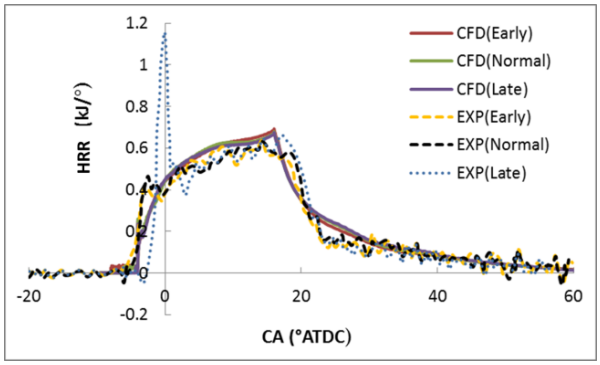

Figure 2. Comparison of HRRs between the experiment (taken from Imhof et al.[2] and the CFD model for three different pilot fuel injection timings in the RCEM chamber.

delayed due to the high dissipation rate and the lack of oxygen content within the ignition kernel, caused by the high-speed gas injection and the high concentration of gas fuel. The pilot fuel continuously accumulates, followed by the extremely rapid combustion in the rich fuel mixture. The respective experimental HRR shown in Figure 2 depicts that the ignition delay of the pilot fuel is apparently prolonged and a high peak of the HRR is obtained. Due to the separate modelling of the pilot fuel and the main gas non-premixed combustion processes, such strong interaction between the main gas and pilot fuels cannot be captured by the employed CFD models.

Table 1. Comparison of NO emissions [in ppm] for the dual fuel and diesel modes in RCEM chamber.

Modes	Developed CFD models	Experiments [2]
`Diesel`	648	531
`DF`	244	346-393
`Early(DF)`	111	223
`Normal(DF)`	105	216
`Late(DF)`	104	260

Parametric Investigation

Aiming to obtain the recommended settings of the gas fuel injection for the investigated marine two-stroke dual fuel HPDI engine operating in the gas mode (with minimum pilot fuel according to the engine manufacturer[9]) at the 75% load,

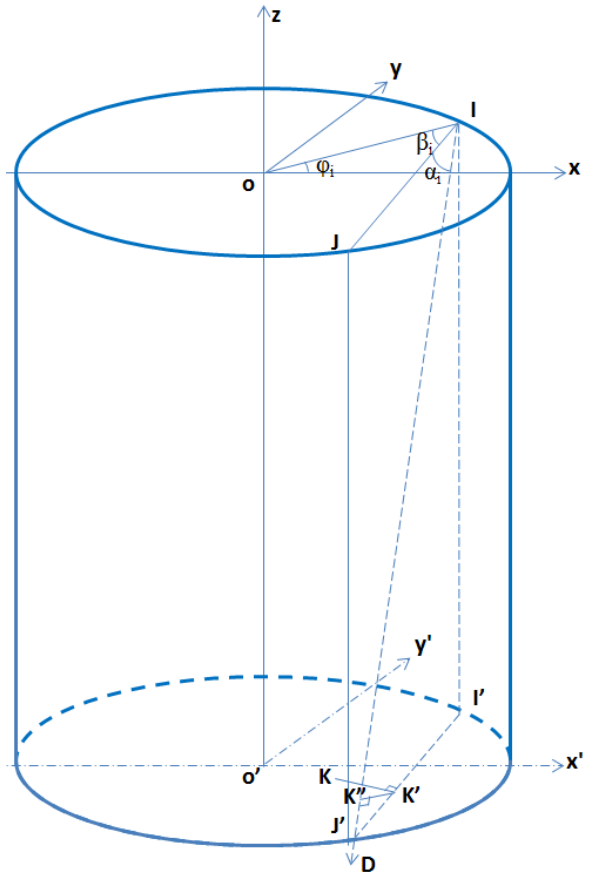

Figure 3. Engine cylinder sketch illustrating the gas injector lateral angle (β_i), the gas injector inclination angle (α_i), and the gas injector location (point I); coordinate z corresponds to the engine cylinder vertical axis.

the parametric investigation of the closed-cycle operation is conducted numerically by using the developed CFD models. The characteristics of the investigated engine[12] are listed in Table 2. The investigated gas injection parameters include the gas injection timing, the gas injection duration, the lateral angle of the gas nozzle (β_i, as shown in Figure 3) and the gas injectors holes number.

Table 2. MAN Diesel & Turbo engine 5S60ME-GI characteristics[9,12].

Parameters	Symbol	Unit	Value
Stroke	S	m	2.4
Bore	B	m	0.6
Crank Radius	R	m	1.2
Engine Speed (75% Load)	N	r/min	91.3
Engine Power(75% Load)	P_B	kW	7875

Effects of the gas injection timing

Table 3 illustrates the pilot fuel and gas fuel injection timing and duration for three investigated cases (DF1-DF3). For the first investigated case (DF1), the injection settings were derived from the pilot fuel injection pressure and the gas injection pressure curves reported by Kjemtrup[10]. The inclination angle of the gas injector was set to 15°, in order to avoid the gas accumulation close to the cylinder head[25]. The other two cases (DF2 and DF3) consider an earlier gas ignition timing at 5.67°CA and 0°CA, respectively.

Table 3. Investigated cases DF1-DF3 settings with different gas fuel injection timings.

Case	Timing (°CA ATDC)	Duration (°CA)	Holes Number (-)	α_i (°)	β_i (°)
DF1	13.81	17.32	1	15	0
DF2	5.67	17.32	1	15	0
DF3	0	17.32	1	15	0

Figure 4 results demonstrate that advancing the gas injection start to the top death center (TDC) (investigated case DF3) can substantially increase the in-cylinder pressure. The cylinder close-cycle indicated mean effective pressure (P_{EC}) (calculated from -7°CA ATDC to 110°CA ATDC) for the DF2 case increases by 14% compared to that of the DF1 case. This is due to the improvement of the gas fuel combustion process, leading to the significant reduction of the incomplete combustion products (carbon monoxide (CO) and unburned hydrocarbons (HC) emissions) as shown in Table 4.

The derived heat release rates (HRRs)[26] for the three investigated cases are presented in Figure 5. Four peaks are observed in the HRRs variations; the three of them are associated with the pilot and the gas fuel combustion. The last peak observed around 40°CA ATDC is attributed to the numerical issues caused by the change of the time step for the decrease of the simulation run computational time. The first valley of the HRR variation is apparently due to the completion of the pilot fuel combustion, whereas the second valley is attributed to the cold gas plumes impinging on the burning gas.

As expected, the improvement of the gas fuel combustion usually implies the higher in-cylinder combustion temperature, which would lead to the increase of the NO emissions. However, the derived NO emissions for the DF2 case are found to be slightly lower than that for the DF1 case. Based on the comparison of the in-cylinder maximum temperature variations and the variations of the high-temperature volume ratio in temperature above 2000 K for the DF1 and DF2 cases (depicted in Figures 6 and 7), it can be inferred that the greater NO emissions for DF1 is primarily attributed to the late continuous gas fuel combustion.

Effects of the gas injection duration

Three cases (DF4, DF5 and DF6) with the gas injection duration varying from 11.24°CA to 17.32°CA are investigated as listed in Table 5.

The results shown in Figure 8 and Table 5 demonstrate that shortening the gas injection duration increases the in-cylinder maximum pressure and the corresponding closed-cycle indicated mean effective pressure, as well as provides a higher pressure rise. This is attributed to the increase of the injected gas mass flow rate and the resulted faster combustion process, due to the reduction of the gas injection duration. Table 6 also indicates that there is no notably change in the intermediate species (CO and HC) produced by the incomplete combustion, which implies that the reduction of

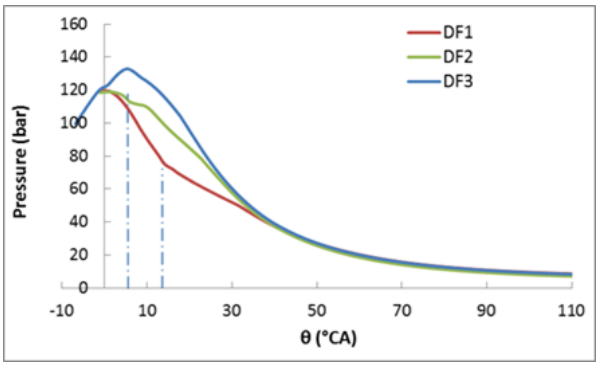

Figure 4. In-cylinder pressure variations for the investigated cases DF1, DF2 and DF3 with different gas injection timings.

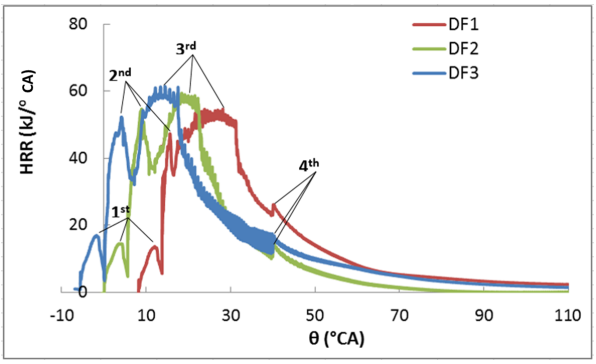

Figure 5. HRR variations for the investigated cases DF1, DF2 and DF3 with different gas injection timings.

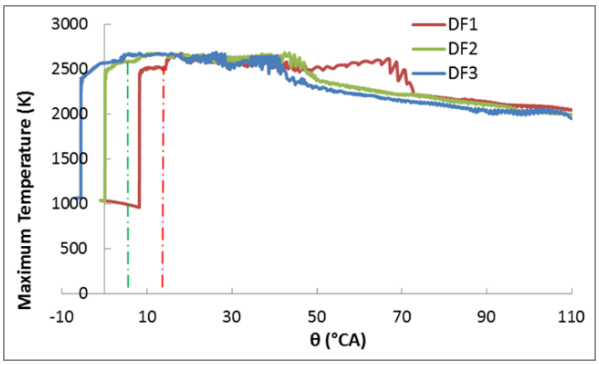

Figure 6. In-cylinder maximum temperature variations for the investigated cases DF1, DF2 and DF3 with different gas injection timings.

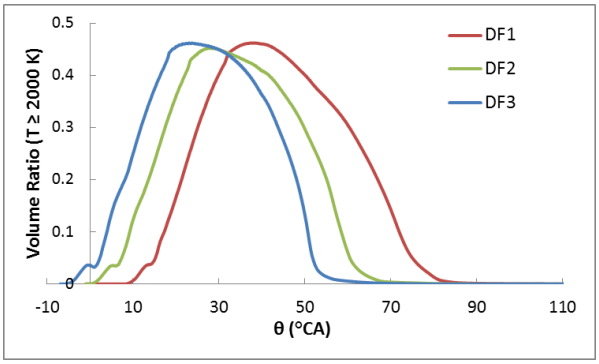

Figure 7. In-cylinder high-temperature (above 2000 K) volume ratio variations for the investigated cases DF1, DF2 and DF3 with different gas injection timings.

Table 4. Calculated engine performance and emissions parameters for the DF1, DF2 and DF3 cases with different gas fuel injection timings.

Case	P_{EC} (MPa)	NO mass fraction (10^{-6})	CO mass fraction (10^{-6})	HC mass fraction (10^{-6})	CO_2 mass fraction (10^{-6})
DF1	1.980	986	11526	304	54796
DF2	2.056	839	10641	211	54557
DF3	2.250	1109	5089	76	56251

Note: Emissions evaluated at 110°CA ATDC before the exhaust valve open;
$P_{EC} = \frac{\int_{-7^\circ CA}^{110^\circ CA} \tilde{P} dV}{\Omega_S}$;
$\tilde{P}$: Cylinder pressure;
V: Cylinder volume;
Ω_S: Cylinder displacement volume.

the gas injection duration and the resultant increase of the gas flow rate do not remarkably improve the gas fuel combustion quality and emissions.

Apparently, the greater cylinder pressure caused by the higher availability of the prepared gas–air mixture leads to a greater in-cylinder mean temperature and heat release rate during the gas injection period, as shown in Figure 9. The considerable reduction of the released heat taking place after the early stage of gas fuel burning at around 6°CA is attributed to the contact of the cold gas plumes with the flame surface.

The three investigated cases (DF4, DF5 and DF6) almost exhibit the same NO emissions, as inferred from the results presented in Table 6, where the maximum difference between the three cases is about 5% . The NO formation is associated with the high-temperature zone within the engine cylinder. The DF6 case with the shortest gas injection duration exhibits the greater maximum temperature in the late combustion phase around 40–50°CA, as shown in Figure 10. With respect to the volume occupied by the gas zone with the temperature greater than 2000 K, only slightly changes can be observed in the results of Figure 11.

Table 5. Investigated cases DF4-DF6 settings with different gas fuel injection duration periods.

Case	Timing (°CA ATDC)	Duration (°CA)	Holes Number (-)	α_i (°)	β_i (°)
DF4	0	17.32	1	15	0
DF5	0	14.46	1	15	0
DF6	0	11.24	1	15	0

Effects of the Single-Hole Gas Injector Lateral Angle

In order to avoid the extended contact of the injected gas stream with the diffusion flame surface, three cases (DF6, DF7 and DF8) for the single-hole gas injector with the different lateral angles are investigated, the parameters of which are presented in Table 7.

From the in-cylinder pressure variations presented in Figure 12, it could be deduced that the change of the

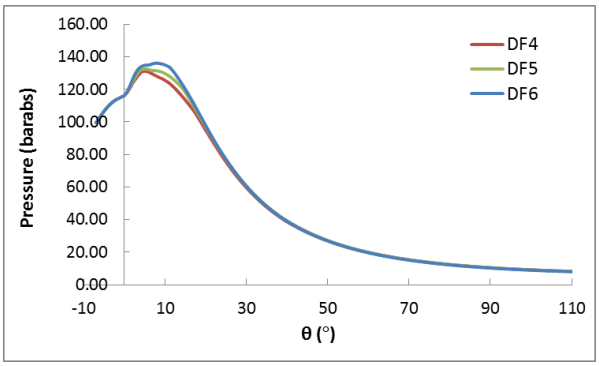

Figure 8. In-cylinder pressure variation for the investigated cases DF4, DF5 and DF6 with different gas injection duration periods.

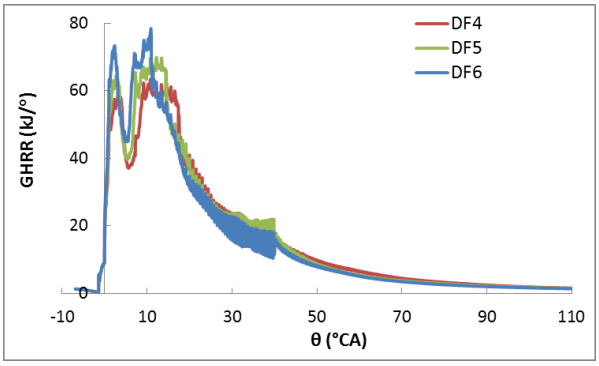

Figure 9. HRR curves for the investigated cases DF4, DF5 and DF6 with different gas injection duration periods.

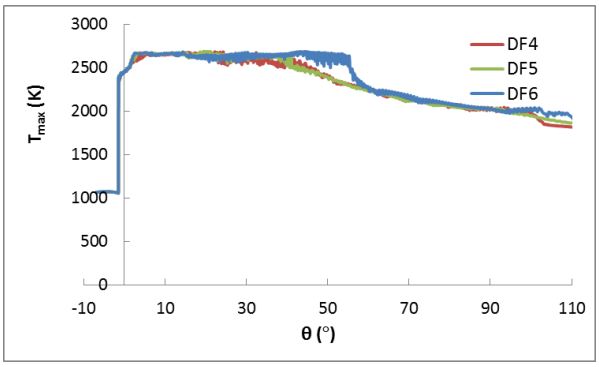

Figure 10. Maximum temperature variation for the investigated cases DF4, DF5 and DF6 with different gas injection duration periods.

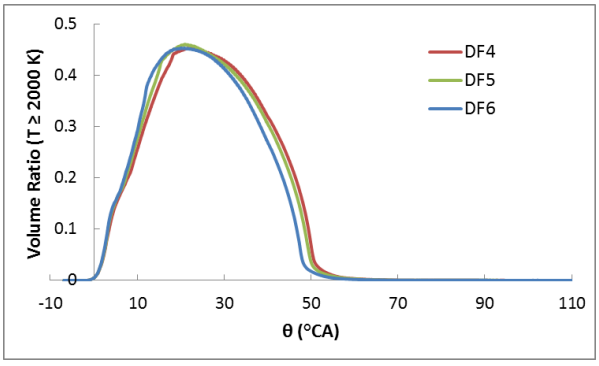

Figure 11. High-temperature volume ratio in-cylinder greater than 2000 K for the investigated cases DF4, DF5 and DF6 with different gas injection duration periods.

Table 6. Calculated engine performance and pollutant emissions for the DF4, DF5 and DF6 cases with different gas fuel injection duration periods.

Case	P_{EC} (MPa)	NO mass fraction (10^{-6})	CO mass fraction (10^{-6})	HC mass fraction (10^{-6})	CO_2 mass fraction (10^{-6})
DF4	2.230	1008	5938	149	69026
DF5	2.261	1059	5994	126	69541
DF6	2.262	1046	6013	120	68402

gas injection direction significantly affects the mean in-cylinder pressure. In addition, the corresponding closed-cycle indicated mean effective pressure increases by 12% as the lateral angle of gas injector varies from 0° to -30° as shown in Table 8. The increase of the in-cylinder pressure is attributed to the improvement of the combustion quality. The HRR curves shown in Figure 13 demonstrate the improvement of the gaseous fuel combustion process, as greater heat release rates were obtained for the investigated cases with a larger gas injector lateral absolute angle.

From Table 8 results, it is deduced that the unburned hydro-carbon (HC) emissions reduce as the gas injector lateral angel absolute value increases. As expected, more CO_2 emissions and less intermediates are produced as the lateral angle of the gas nozzle changes to -30° in comparison with the cases with the smaller gas injector lateral angle absolute values.

From Figure 14, it can be deduced that the period with the maximum temperature around 2600 K is shortened in the DF6 case, which is attributed to the reduction of the intermediates dwelling in the cylinder. However, the NO emissions substantially increase, as indicated in Table 8. This is owing to the fact that the combustion chamber volume with the temperature greater than 2400 K significantly increases, as illustrated in Figure 15.

Table 7. Investigated cases DF6-DF8 gas injection settings with different gas injector lateral angles.

Case	Timing (°CA ATDC)	Duration (°CA)	Holes Number (-)	α_i (°)	β_i (°)
DF6	0	11.24	1	15	0
DF7	0	11.24	1	15	-15
DF8	0	11.24	1	15	-30

Table 8. Calculated engine performance and emissions for the DF6, DF7 and DF8 cases with different gas injector lateral angles.

Case	P_{EC} (MPa)	NO mass fraction (10^{-6})	CO mass fraction (10^{-6})	HC mass fraction (10^{-6})	CO_2 mass fraction (10^{-6})
DF6	2.262	1046	6013	120	68402
DF7	2.458	1864	1419	8	77596
DF8	2.524	2282	18	0	79765

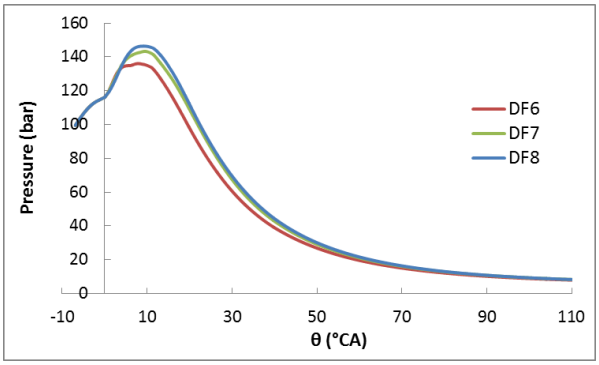

Figure 12. In-cylinder pressure variation for the investigated cases DF6, DF7 and DF8 with different gas injector lateral angles.

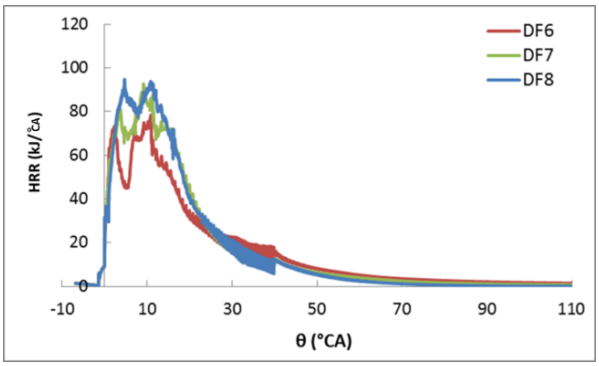

Figure 13. HRRs variations for the investigated cases DF6, DF7 and DF8 with different gas injector lateral angles.

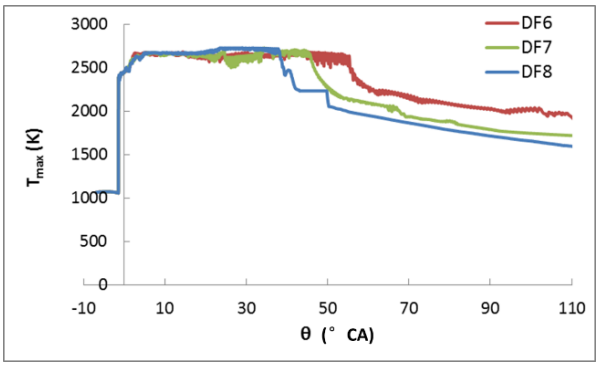

Figure 14. Maximum temperature for the investigated cases DF6, DF7 and DF8 with different gas injector lateral angles.

Effects of the Gas Injector Holes Number

Three types of gas injectors with one, three and five holes are investigated (cases DF8, DF9 and DF10, respectively). The lateral angle of the middle hole in each gas injector is -30°, whereas the separation angle between holes is considered to be 20°. The gas injectors settings for the three investigated cases are illustrated in Table 9.

The results presented in Figures 16 and 17 demonstrate that the relationship between the gas injector holes number, the HRRs and the in-cylinder pressure is not monotonous. The greatest heat release peak values caused by the fastest gas fuel burning rate (Figure 17) were obtained for the DF10 case with the largest number of gas injector holes. This resulted in the greatest in-cylinder maximum pressure values and the lowest in-cylinder pressure during the late combustion process period as well as the fastest CO_2 production (Figure 18). The results presented in Figure 19 demonstrate that the mixing process for the DF10 case with

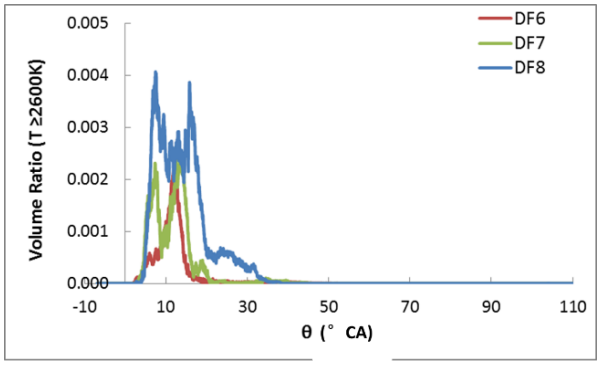

(a) Temperature greater than 2600 K

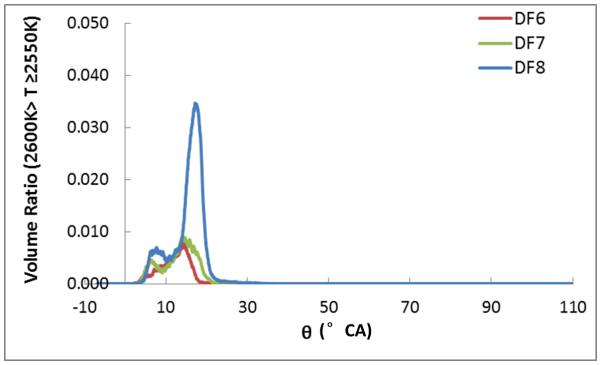

(b) Temperature between 2550 K and 2600 K

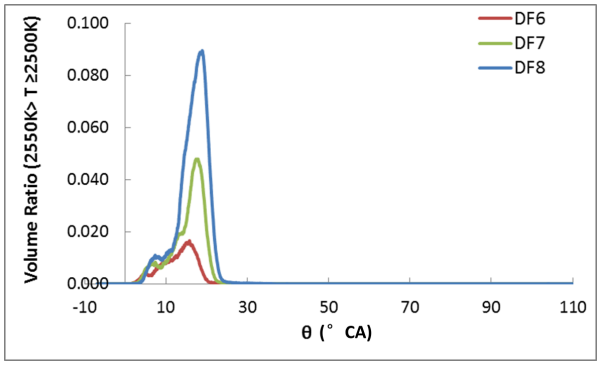

(c) Temperature between 2500 K and 2550 K

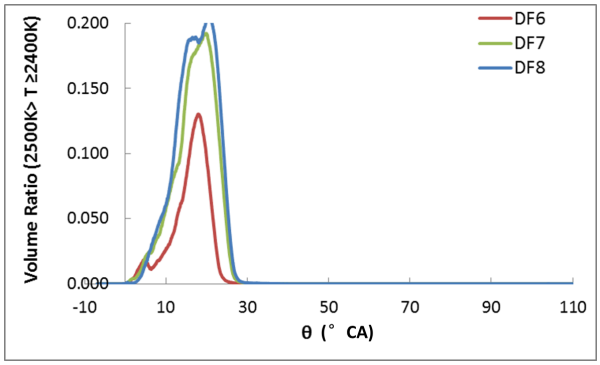

(d) Temperature between 2400 K and 2500 K

Figure 15. High-temperature volume ratio greater 2000 K for the investigated cases DF6, DF7 and DF8 with different gas injector lateral angles.

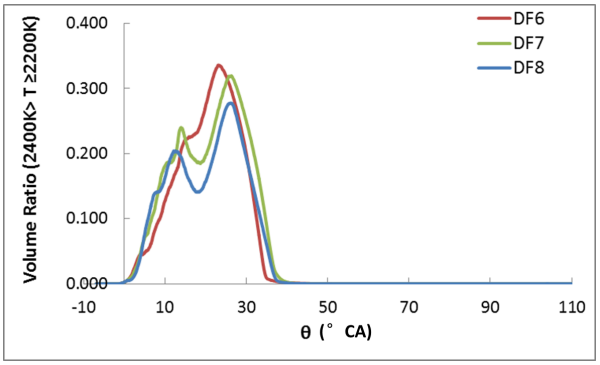

(e) Temperature between 2200 K and 2400 K

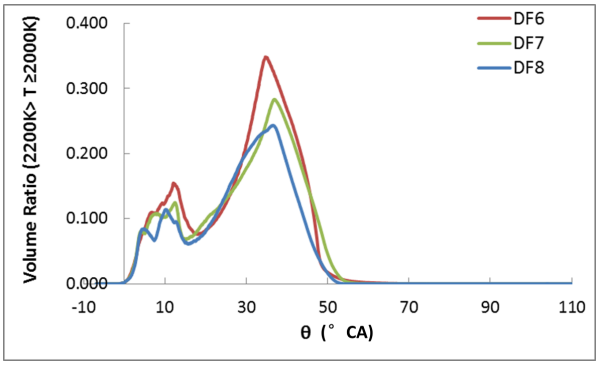

(f) Temperature between 2000 K and 2200 K

Figure 15. High-temperature volume ratio greater 2000 K for the investigated cases DF6, DF7 and DF8 with different gas injector lateral angles.

the 5-hole gas injector is more effective in comparison with the ones of other two investigated cases.

According to the results presented in Table 10, the closed-cycle indicated mean effective pressure for the DF10 case is found to be 3% lower than that of the DF8 case, despite the higher peak pressure for the latter. For the three investigated cases, Table 10 results demonstrate that all the methane is consumed and the unburned HC and CO emissions are extremely low, due to the very efficient combustion process.

In addition, the investigated case DF8 with the single hole gas injector exhibited the greatest NO emissions (Table 10). This is attributed to the greater maximum temperature values and the flame volume during the gas combustion process, as it can be deduced from the results presented in Figures 20 and 21. The minimum NO emissions are obtained for the DF9 case, but the closed-cycle indicated mean effective pressure is also considerably reduced in this case. According to the derived HRRs and the flame temperature variations shown in Figures 17 and 20, the reduction of the in-cylinder pressure for DF9 is mainly due to the late gas fuel combustion. A remarkable reduction of NO emissions by 23% is derived for the DF10 case, whilst maintaining a similar power level with the DF8 case (as inferred comparing the respective values of the closed-cycle indicated mean effective pressure).

Recommended settings of the gas injection parameters

The derived results for the NO and CO_2 emissions versus the indicated mean effective pressure of the closed cycle (P_{EC})

Table 9. Investigated cases DF8-DF10 gas injection settings with different gas injector holes numbers.

Case	Timing (°CA ATDC)	Duration (°CA)	Holes Number (-)	α_i (°)	β_i (°)
DF8	0	11.24	1	15	-30
DF9	0	11.24	3	15	-50,-30,-10
DF10	0	11.24	5	15	-70,-50, -30,-10,10

Table 10. Calculated engine performance and emissions for the DF8, DF9 and DF10 cases with different gas injector holes numbers.

Case	P_{EC} (MPa)	NO mass fraction (10^{-6})	CO mass fraction (10^{-6})	HC mass fraction (10^{-6})	CO_2 mass fraction (10^{-6})
DF8	2.524	2282	18	0	79765
DF9	2.399	1260	13	0	79841
DF10	2.450	1791	6	0	79457

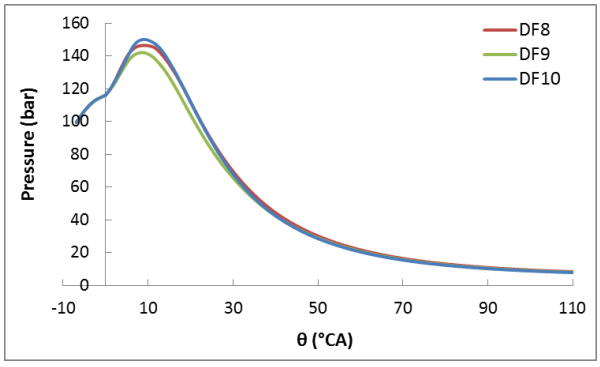

Figure 16. In-cylinder pressure variations for the investigated cases DF8, DF9 and DF10 with the different gas injector holes numbers.

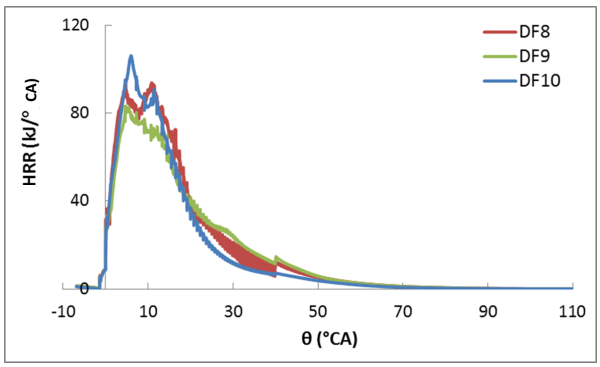

Figure 17. HRR variations for the investigated cases DF8, DF9 and DF10 with the different gas injector holes numbers.

for all the investigated cases (DF1-DF10) are plotted in Figure 22. In order to maintain the same engine output with the diesel mode, the settings of the DF7, DF8, DF10 cases can potentially be selected. By comparing the emissions in these selected three cases, it can be observed that the lowest CO_2 and NO emissions are obtained for the DF10 case (reductions of 0.4% and 12% were estimated for the NO and

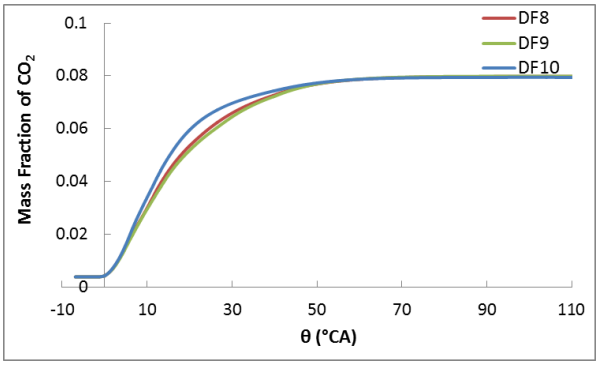

Figure 18. Mass fraction of carbon dioxide for the investigated cases DF8, DF9 and DF10 with the different gas injector holes numbers.

CO_2, respectively in comparison with the DF8 case). In this respect, the gas injection parameters of the DF10 case are recommended for the investigated engine operation in the gas mode (with the minimum pilot fuel according to the engine manufacturer[9]) at 75% load.

In order to compare the power output of the investigated engine operating in the gas and diesel modes, the full engine cycle of one engine cylinder was simulated at 75% load in both operating modes by employing the developed CFD model. To simulate the engine open cycle processes (which include the exhaust blowdown and the scavenging processes), the exhaust valve lift profile and the scavenging ports opening/closing profile were provided as input. The developed CFD model in the ANSYS Fluent software[13] was set up to automatically activate/deactivate the domains representing the exhaust port and the scavenge air box based on the crank angle, as well as to adjust the simulation time step accordingly.

The derived CFD model results for the in-cylinder pressure variation and the HRRs are presented in Figure 23 and 24. The experimentally measure cylinder pressure diagram for the diesel mode operation taken from Jin[27] is also presented in Figure 23. It can be deduced from Figure 23 results, that the CFD model predicted in-cylinder pressure variation for the diesel mode operation almost coincides with the respective experimentally measured one. For the diesel mode, the difference of the calculated full-cycle indicated mean effective pressure from the CFD results and the measured values is within 0.1% (despite of the slightly underestimation by 1.8% of the in-cylinder maximum pressure in the case of the CFD model calculations). In this respect, it can be inferred that the CFD model results are of adequate accuracy.

Based on the cylinder pressure variations for the gas and the diesel modes shown in Figure 23, it can be inferred that the difference in calculated full-cycle indicated mean effective pressures for these two modes is lower than 0.1% . Therefore, it can be concluded that that the recommended injection settings employed for the gas operating mode at 75% load render the investigated engine to retain the diesel mode power output (at the same load conditions).

The heat release rate (HRR) for the gas mode is remarkably different than that of the diesel mode, as shown in Figure 24. For the diesel operation, the valley between the two HRR peaks is attributed to the less fuel vapour retained in the engine combustion chamber[11]. The HRR for the gas mode reaches its maximum value at 5.62°CA ATDC; the

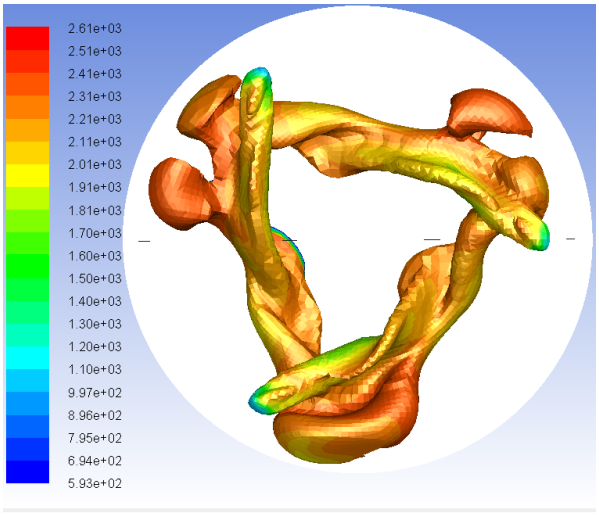

(a) Single-hole gas injector

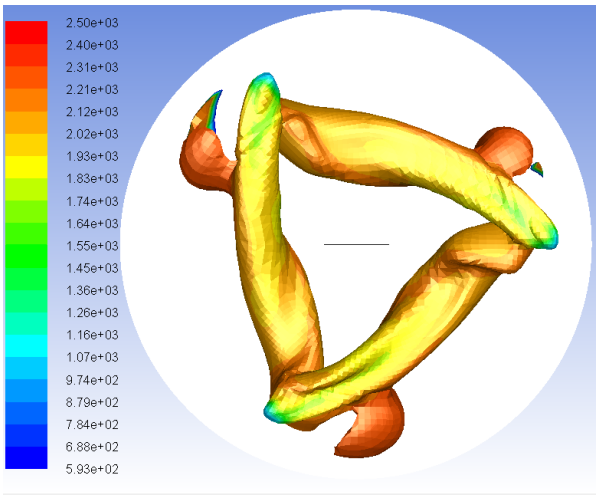

(b) Three-hole gas injector

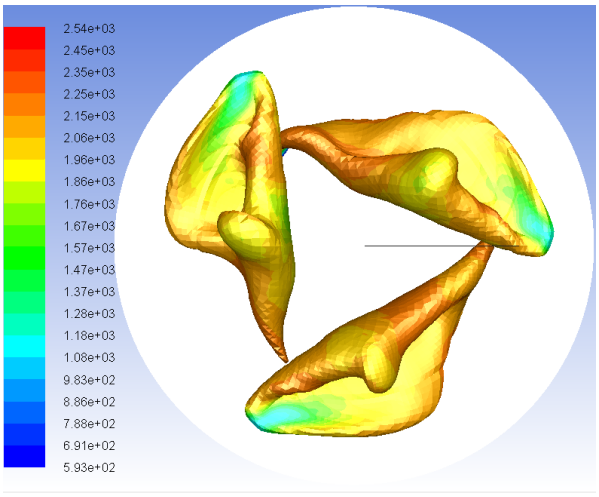

(c) Five-hole gas injector

Figure 19. The temperature contours on the stoichiometric surface of the gas plumes at crank angle 10°CA ATDC for the investigated cases DF8, DF9 and DF10 with different gas injector holes number.

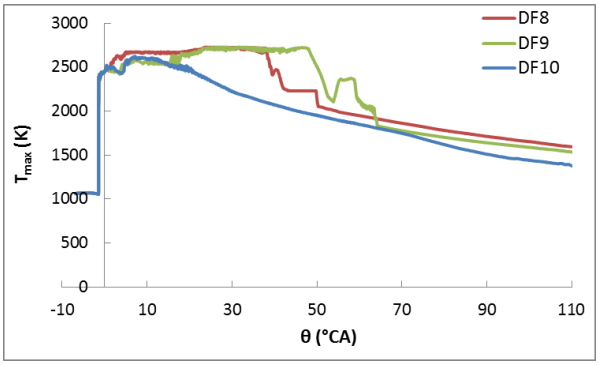

Figure 20. In-cylinder maximum temperature variations for the investigated cases DF8, DF9 and DF10 with different gas injector holes number.

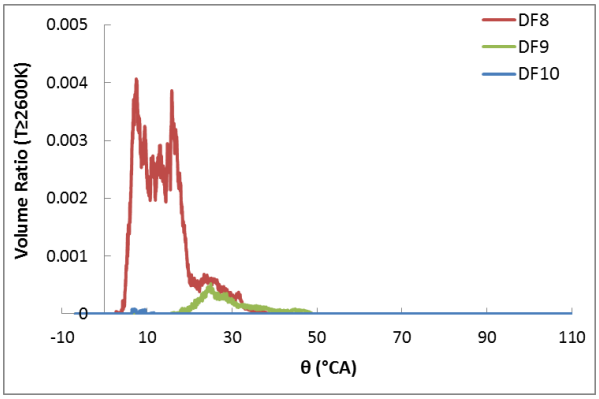

(a) Temperature greater than 2600 K

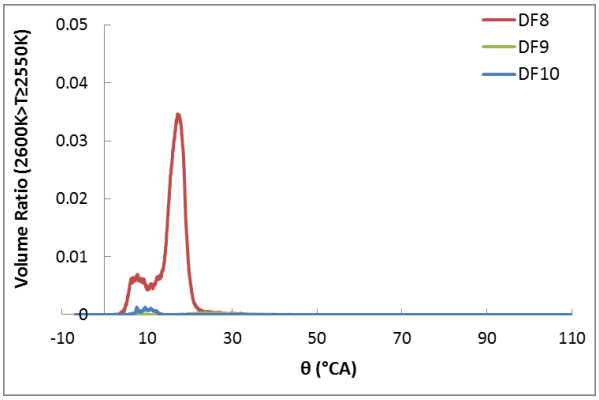

(b) Temperature between 2550 K and 2600 K

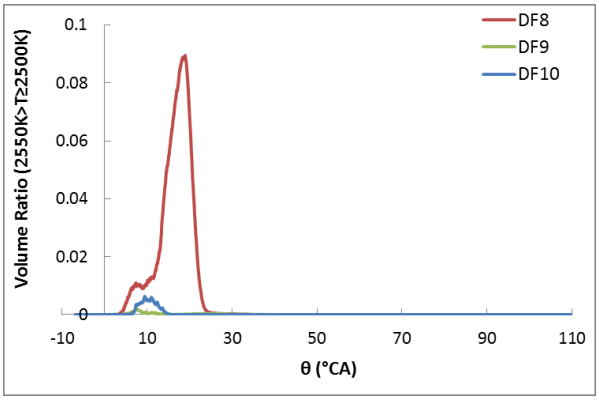

(c) Temperature between 2500 K and 2550 K

Figure 21. High-temperature volume ratio greater 2000 K for the investigated cases DF8, DF9 and DF10 with different gas injector holes number.

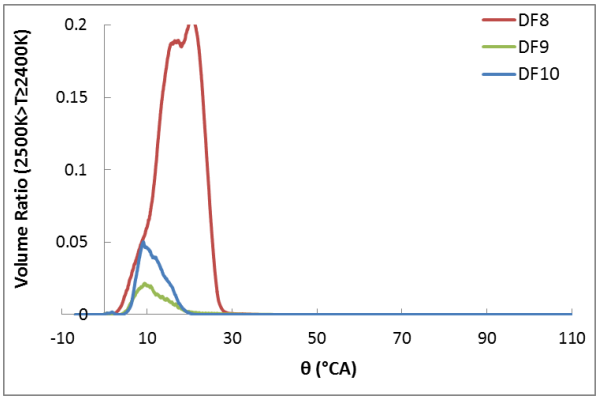

(d) Temperature between 2400 K and 2500 K

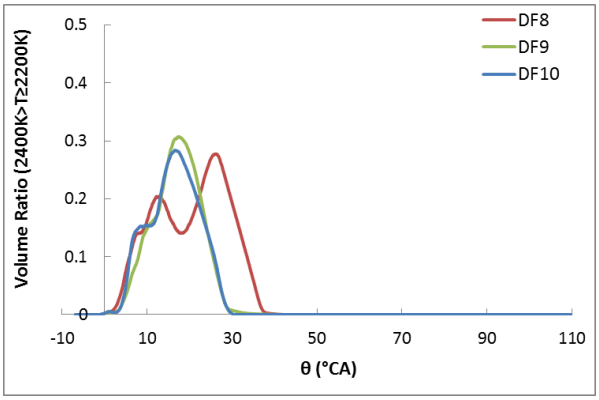

(e) Temperature between 2200 K and 2400 K

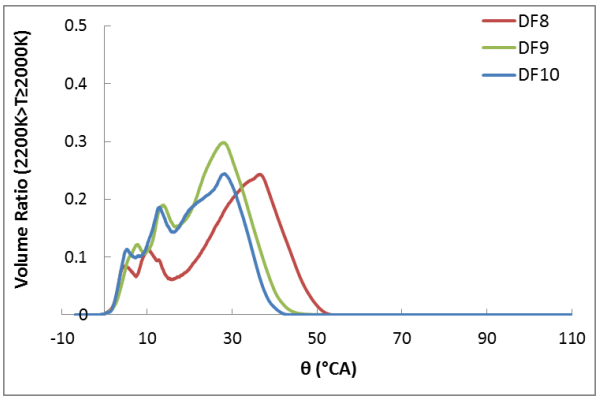

(f) Temperature between 2000 K and 2200 K

Figure 21. High-temperature volume ratio greater 2000 K for the investigated cases DF8, DF9 and DF10 with different gas injector holes numbers.

gradual decrease of the HHR variation follows the peak value point .

Table 11 indicates that the CO_2 and NO emissions for the gas mode are lower of 21% and 31% respectively than the ones estimated for the diesel mode. The HC emissions are almost eliminated in both operation modes, which coincides with the literature findings for the HPDI engine types (considerable NOx emissions and very low HC emissions).

Conclusions

The parametric investigation of the large marine two-stroke dual fuel engine of the high pressure direct injection (HPDI) type was conducted for the gas mode (with minimum pilot

Table 11. Calculated emissions by the CFD model for engine operation in the gas and diesel modes at 75% load.

Operating Mode	HC mass fraction (10^{-6})	CO_2 mass fraction (%)	NO mass fraction (10^{-6})
Gas mode	0.0	7.95	1820
Diesel mode	0.0	9.96	2622

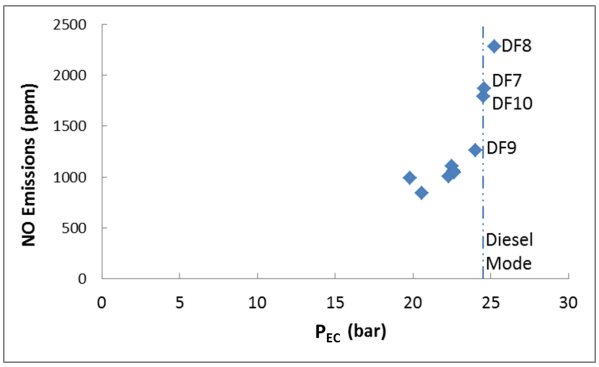

(a) NO emissions versus P_{EC}

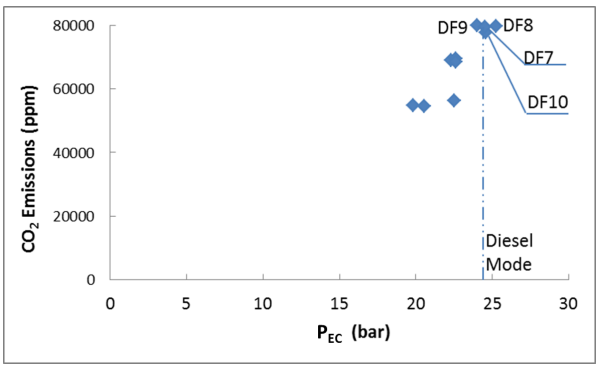

(b) CO_2 emissions versus P_{EC}

Figure 22. NO and CO_2 emissions versus the closed-cycle indicated mean effective pressure (P_{EC}) for all the investigated cases (DF1 to DF10) .

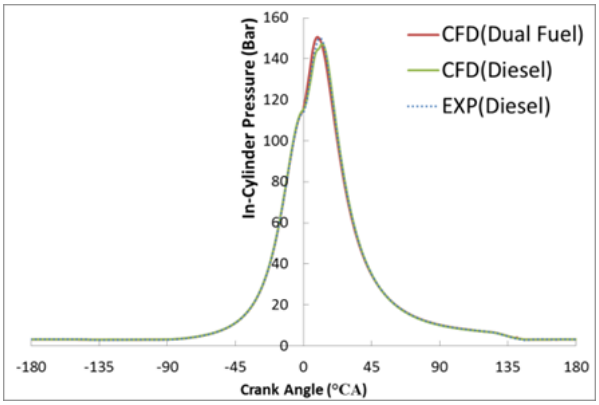

Figure 23. In-cylinder pressure variations in the complete cycle for the investigated engine operation in the gas mode (denoted as Dual Fuel in the legend) and the diesel mode at 75% load.

fuel) operation at 75% load. One cylinder of the 5S60ME-GI engine was simulated by employing a CFD model developed in the ANSYS Fluent software, which utilises sub-models

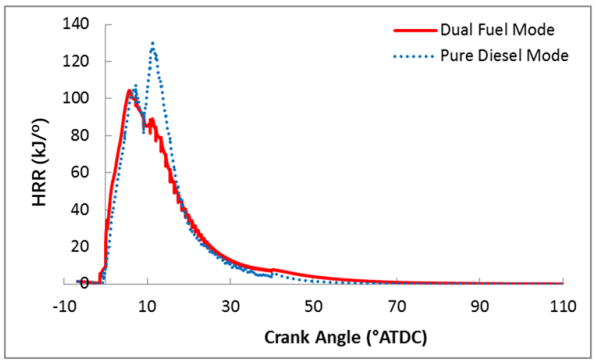

Figure 24. HRR variations calculated by the CFD model for the investigated engine operation in the gas mode (denoted as Dual Fuel in the legend) and the diesel mode at 75% load.

and domains for representing both the closed-cycle and the full-cycle processes. The following settings for the gas fuel injection were investigated: the gas injection timing, the gas injection duration, the gas injector holes number, and the gas injector direction. The recommended settings were identified by considering the close-cycle indicated mean effective pressure, the heat release rates as well as the NO and CO_2 emissions. The full-cycle was simulated for the cases of the gas operating mode with the recommended settings and the diesel operating mode, so that the engine performance and emissions parameters are compared and discussed.

The main findings of this study are summarised as follows.

(i) The most sensitive parameter from the investigated gas injection settings was found to be the gas injector lateral angle. Changes of the gas injector lateral angle from 0° to -30° resulted in a considerable improvement of the gaseous fuel combustion process; in specific, increased the closed-cycle indicated mean effective pressure by 12% substantially increased the NO and CO_2 emissions as well ad reduced the HC emissions.

(ii) For satisfying the contradictory objectives of retaining the engine power and reducing the NO and CO_2 emissions, the gas injection parameters of the DF10 case were recommended for the investigated engine operating in the the gas mode at 75% load.

(iii) The engine operation with the recommended injection settings in the gas mode at 75% load exhibited the same power output with the diesel mode operation; however the carbon dioxide and the nitrogen monoxide emissions for the gas mode were found to be 21% and 31% lower than the ones of the diesel mode, respectively.

In conclusion, the developed CFD model as well as the results of this study can remarkably beneficial for reducing the effort required to optimise the engine settings in the other engine loads. The developed CFD method is expected to be a useful tool and can be employed during the engine design phase as: (a) it provides advantages on investigating the engine cycle physical phenomena and capturing the complicated physics of the involved processes; (b) the engine performance and emissions strongly depend on the engine components design, the engine systems settings and

the engine operating conditions; and (c) it is extremely challenging and costly to directly acquire measurements (apart from the in-cylinder pressure) that can be employed for characterising the engine in-cylinder processes.

The following areas are proposed for the future investigation of the large marine two-stroke dual fuel engines:

(i) Optimisation of the gas injection parameters in other engine loads with the objectives to retain the engine power and reduce the NO and CO_2 emissions.
(ii) Various gas fuels with different characteristics, their skeletal chemical mechanisms as well as their effects on the engine combustion process.
(iii) Other fuels including bio-diesel, methanol, bio-gas, and synthetic fuel, as well as their chemical mechanisms.

Acknowledgements

All the CFD simulations presented in the paper were carried out at the ARCHIE-WeSt supercomputers. The authors would like to appreciate the administrators to provide the adequate computational resources to complete this investigation. The authors gratefully acknowledge the financial support of the European Commission through the research project JOULES (Website: http://www.joules-project.eu), which is jointly funded by the 7^th Framework Programme and the industry, for the work reported in this article. The authors from MSRC greatly acknowledge the funding from DNV GL AS and RCCL for the MSRC establishment and operation. The opinions expressed herein are those of the authors and should not be construed to reflect the views of EU, DNV GL AS and RCCL.

References

1. Larson CR. *Injection study of a diesel engine fuelled with pilot-ignited, directly-injected natural gas*. Master Thesis, University of British Columbia, Canada 2003.
2. Imhof D, Tsuru D, Tajima H and Takasaki K. High-pressure natural gas injection (GI) marine engine research with a rapid compression expansion machine. In: 27^{th} *CIMAC World Congress on Combustion Engines*, Shanghai, China, 13-16 May 2013.
3. Lee WG and Montgomery D. Numerical investigation of the performance of a high pressure direct injection (HPDI) natural gas engine. In: *Proceedings of the ASME Internal Combustion Engine Division Fall Technical Conference*, Volume 2: Instrumentation, Controls, and Hybrids; Numerical Simulation; Engine Design and Mechanical Development; Keynote Papers: V002T06A019, Columbus, IN, USA, October 19-22, 2014.
4. Li M, Zhang Q, Li G and Shao S. Experimental investigation on performance and heat release analysis of a pilot ignited direct injection natural gas engine. *Energy* 2015; 90: 1251-1260.
5. Zhang Q, Li M and Shao S. Combustion process and emissions of a heavy-duty engine fueled with directly injected natural gas and pilot diesel. *Applied Energy* 2015; 157: 217–228.
6. Gao Y, et al. Numerical simulations of natural gas injection pressure effects on a direct injected, pilot ignited, natural gas engine. *Applied Mechanics and Materials* 2014; 510: 179-184.
7. Wang Q, Shao C, Liu Q, Zhang Z and He Z. Effects of injection rate on combustion and emissions of a pilot ignited direct injection natural gas engine. *Journal of Mechanical Science and Technology* 2017; 31(4): 1969-1978.
8. Duggal VK, Lyford-Pike EJ and Wright JF. *Development of the high-pressure direct-injected, ultralow-NOx natural gas engine: final report*. Report for National Renewable Energy Laboratory (NREL). Report no. SR-540-35911, 2004. Golden, CO (US).
9. MAN B&W. MAN B&W S60ME-C8.5-GI-TII, project guide - electronically controlled dual fuel two-stroke engines,https://marine.man-es.com/two-stroke/project-guides (2016, accessed 5 May 2016).
10. Kjemtrup N. Gas 2-stroke marine engine design and operation. In: *Greek CIMAC Association Seminar*, Athens, Greece, 22 January 2015.
11. Yang R. *CFD modelling and investigation of the marine dual-fuel two-stroke engine with gas high pressure direct admission*. PhD Thesis, University of Strathclyde, UK, 2018.
12. MAN B&W. CEAS engine data report 5S60ME-C8.5-GI (methane) with high load tuning, http://marine.man.eu/two-stroke/ceas (2016, accessed 5 May 2016).
13. ANSYS Inc. ANSYS Fluent theory guide release 15.0, https://www.ansys.com/ (2015, accessed 7 July 2015).
14. Menter FR. Two-equation eddy-viscosity turbulence models for engineering applications. *AIAA Journal* 1994; 32(8): 1598–1605.
15. Peng DY and Robinson DB. A new two-constant equation of state. *Industrial and Engineering Chemistry: Fundamentals* 1976; 15: 59-64.
16. Apte SV, et al. LES of atomizing spray with stochastic modelling of secondary breakup. *International Journal of Multiphase Flow* 2003; 29: 1503 –1522.
17. Ouellette P and Hill PG. Turbulent transient gas injections. *Journal of Fluids Engineering* 2000; 122: 743.
18. Hajialimohammadi A, et al. Ultra high speed investigation of gaseous jet injected by a singlehole injector and proposing of an analytical method for pressure loss prediction during transient injection. *Fuel* 2016; 184: 100-109.
19. Choi M, Lee S and Park S. Numerical and experimental study of gaseous fuel injection for CNG direct injection. *Fuel* 2015; 140, 693-700.
20. Peters N. Laminar diffusion Flamelet models in non-premixed turbulent combustion. *Prog. Energy Combust. Sci.* 1984; 10: 319-339.
21. Bilger RW and Starner SH. On reduced mechanism for methane-air combustion in nonpremixed flames. *Combustion and Flame* 1990; 80: 135-149.
22. Hanson RK and Salimian S. Survey of rate constants in H/N/O systems. In: Gardiner W.C. (eds) *Combustion Chemistry*. New York: Springer, 1984, pp. 361-421.
23. Schwerdt C. *Modelling NOx-formation in combustion processes*. Master Thesis, Lund University, Sweden, 2006.
24. Tao F, Reitz RD, Foster DE and Liu Y. Nine-step phenomenological diesel soot model validated over a wide range of engine conditions. *Int. J. Therm. Sci.* 2007; 48: 1223–1234.
25. Yang R, Theotokatos G and Vassalos D. Numerical investigation of the gas injection process in large marine DF

engines. In: *International Conference on Maritime Safety and Operations*, Glasgow, UK, 13 – 14 October, 2016.

26. Papagiannakis RG and Hountalas DT. Experimental investigation concerning the effect of natural gas percentage on performance and emissions of a DI dual fuel diesel engine. *Applied Thermal Engineering* 2003; 23: 353-365.
27. Jin W. *CFD modelling and validation of a large 2-stroke marine diesel engine*. PhD Thesis, University of Strathclyde, UK, 2014.